AGU Advances

RESEARCH ARTICLE
10.1029/2020AV000303

Urban Forests as Main Regulator of the Evaporative Cooling Effect in Cities

Athanasios Paschalis[1], TC Chakraborty[2], Simone Fatichi[3], Naika Meili[4,5], and Gabriele Manoli[6]

[1]Department of Civil & Environmental Engineering, Imperial College London, UK, [2]Yale School of the Environment, Yale University, USA, [3]Department of Civil & Environmental Engineering, National University of Singapore, Singapore, [4]Future Cities Laboratory, Singapore-ETH Centre, Singapore, [5]Institute of Environmental Engineering, ETH Zurich, Switzerland, [6]Department of Civil, Environmental & Geomatic Engineering, University College London, UK

Key Points:

- Urban vegetation explains the largest fraction of the surface urban heat island (UHI) variability
- Urban vegetation type explains the dependence of surface UHI intensity to background climate
- Maintaining natural reserves in cities effectively mitigates UHIs

Supporting Information:

Supporting Information may be found in the online version of this article.

Correspondence to:

A. Paschalis,
a.paschalis@imperial.ac.uk

Citation:

Paschalis, A., Chakraborty, T., Fatichi, S., Meili, N., & Manoli, G. (2021). Urban forests as main regulator of the evaporative cooling effect in cities. *AGU Advances*, *2*, e2020AV000303. https://doi.org/10.1029/2020AV000303

Received 17 SEP 2020
Accepted 22 MAR 2021

Author Contributions:

Conceptualization: Simone Fatichi, Gabriele Manoli
Data curation: TC Chakraborty
Methodology: Simone Fatichi, Naika Meili, Gabriele Manoli
Writing – original draft: Simone Fatichi, Naika Meili, Gabriele Manoli
Writing – review & editing: TC Chakraborty, Simone Fatichi, Naika Meili, Gabriele Manoli

Abstract Higher temperatures in urban areas expose a large fraction of the human population to potentially dangerous heat stress. Green spaces are promoted worldwide as local and city-scale cooling strategies but the amount, type, and functioning of vegetation in cities lack quantification and their interaction with urban climate in different settings remains a matter of debate. Here we use state-of-the-art remote sensing data from 145 city clusters to disentangle the drivers of surface urban heat islands (SUHI) intensity and quantify urban-rural differences in vegetation cover, species composition, and evaporative cooling. We show that nighttime SUHIs are affected mostly by abiotic factors, while daytime SUHIs are highly correlated with vegetation characteristics and the wetness of the background climate. Magnitude and seasonality of daytime SUHIs are controlled by urban-rural differences in plant transpiration and leaf area, which explain the dependence of SUHIs on wetness conditions. Leaf area differences are caused primarily by changes in vegetation type and a loss of in-city forested areas, highlighting the importance of maintaining "natural reserves" as a sustainable heat mitigation policy.

Plain Language Summary More than half of the world's population currently lives in cities. Large cities are exposed to higher temperatures than their surrounding rural areas, a phenomenon known as the Urban Heat Island (UHI). Greening our cities has been proposed as an effective Urban Heat mitigation strategy. However, a detailed global scale quantification of the effect of urban vegetation to urban microclimate remains an open debate. The reason for that has been traditionally been the lack of global scale data needed to describe the urban form, and how plants operate within in. In this study, we used the last generation satellite data to quantify all those factors. Utilizing those data, we found that urban vegetation is the most important factor regulating UHI intensities globally. Most importantly we found that the type of vegetation (urban forest or urban grasslands) play a major role in explaining the development or UHIs.

1. Introduction

With the global population increasingly living in cities (e.g., Seto et al., 2011), urban vegetation can provide critical ecosystem services for human and ecological well-being (Endreny, 2018) for a large fraction of the global population. Urban green spaces, such as parks, gardens, and street trees, represent such a "natural capital" for cities (Willis & Petrokofsky, 2017). In addition to other co-benefits (Fong et al., 2018; Z. Zhang et al., 2021), a crucial ecosystem service that green infrastructure can provide is the amelioration of urban climate (e.g., Winbourne et al., 2020), which is an urgent need for urban dwellers coping with the risk of extreme heat stress associated with global climate change (e.g., Raymond et al., 2020) and the urban heat island (UHI) effect (e.g., Manoli et al., 2019). While the ability of urban vegetation to reduce air and surface temperature is well known at the local scale (e.g., Winbourne et al., 2020), the heterogeneity of cities and the global variability of background climate, land management strategies, and vegetation characteristics, make it difficult to arrive at general conclusions on the cooling effect of city-scale strategies aimed at increasing green cover. The spatial extent of vegetated surfaces clearly plays a role in reducing urban temperatures (e.g., Manoli et al., 2019; Winbourne et al., 2020), but the different amount and type of green spaces in existing cities and the various interactions among vegetation type, phenology, and UHI intensity remain largely unexplored.

UHIs are urban-rural differentials of air and surface temperature known as canopy UHI (CUHIs hereinafter) and surface UHIs (SUHIs hereinafter), respectively (T. R. Oke et al., 2017). Due to the availability of satellite observations, SUHIs have been extensively documented globally (e.g., Chakraborty & Lee, 2019; Manoli et al., 2019; Peng et al., 2012; Stewart, 2011; K. Ward et al., 2016), while CUHIs are generally studied for individual cities only (Stewart, 2011). CUHIs and SUHIs exhibit distinct diurnal patterns (the former are mostly a nighttime phenomenon while the latter generally peak during daytime) but they are tightly connected once averaged daily or over longer timescales (Chakraborty et al., 2017; Sun et al., 2020; Zhou et al., 2019) and represent key metrics to quantify the additional threat of heat exposure posed by global urbanization (e.g., Chakraborty et al., 2020).

UHIs can lead to significant excess mortality during heatwaves (e.g., Heaviside et al., 2016; Tan et al., 2010) and simultaneously increase energy costs due to building cooling requirements (e.g., Kolokotroni et al., 2012; Santamouris, 2014). The problem is expected to be exacerbated in the future due to increasing likelihood of heat waves (e.g., Murari et al., 2015; Schoetter et al., 2015; Zhao, 2018), which, in combination with UHIs, will expose urban population to an unprecedented heat risk (D. Li & Bou-Zeid, 2013; Raymond et al., 2020). Hence, considering the combined risks of climate change, UHI development (e.g., Zhao et al., 2018), and increasing exposed population (e.g., Angel et al., 2011; Chen et al., 2020), there is an urgent need to quantify the drivers of urban-induced warming and develop efficient, geographically targeted, mitigation strategies, such as urban greening (Manoli et al., 2019).

The energetics of the UHI have long been investigated (e.g., Howard, 1833; T. Oke, 1982) and over time, our quantitative understanding of the causes of UHIs has significantly improved (e.g., Arnfield, 2003; Mills, 2014; T. R. Oke et al., 2017). Important factors leading to high UHI intensities, especially during night, include heat emitted by buildings and from various anthropogenic activities adding a significant amount of excess heat, particularly in large busy cities (e.g., Allen et al., 2011). Additionally, the urban fabric affects the land-surface's roughness and thus turbulent exchanges (e.g., Rotach, 1999). During daytime both CUHIs and SUHIs are influenced by the lower evapotranspiration in cities (Zhao et al., 2014; Ziter et al., 2019). Due to their impervious surfaces and relative lack of vegetation, cities on average have much higher Bowen ratios (sensible to latent heat ratios) in comparison to the nearby rural areas, though both are exposed to the same regional climate. Increased Bowen ratios result in higher surface temperatures, which can also influence near-surface temperatures.

Hence, lowering the Bowen ratio of cities, is an attractive strategy to reduce urban warming. Since plant transpiration contributes to the largest fraction of the latent heat flux (e.g., Paschalis et al., 2018), urban greening has been widely recognized as an effective strategy for improving microclimate and reducing UHIs (e.g., Gunawardena et al., 2017). Satellite imagery (Figure 1b–1g) clearly shows that green urban areas with high photosynthetic rates and thus high evaporative cooling via transpiration coincide with low surface temperatures. However, quantification of the importance of plant transpiration for UHI mitigation is far from trivial. Urban vegetation commonly consists of nonnative species (e.g., Avolio et al., 2018), is heavily managed, and, being within the city, is exposed to a different microclimate than native vegetation or crops in the nearby rural areas. Considering that vegetation responses to climate are species specific (e.g., Pappas et al., 2016) and vegetation is patchy in cities, it has been a major challenge to quantify latent heat fluxes in urban environments. Latent heat fluxes have also been found to have the largest discrepancy among urban canopy models and between models and measurements (Grimmond et al., 2010). Such a challenge has also likely limited our capacity to bring quantitative criteria in the design of urban greening, including species selection.

The data required to disentangle the relative contributions of background climate, urban fabric, vegetation structure and its evaporative cooling effect (D. Li et al., 2019; Manoli et al., 2019; Zhao et al., 2014), have traditionally been a crucial limitation. A very high spatial resolution is needed to understand city scale processes, particularly when urban greening is a crucial factor, as urban green spaces often cover small areas and are scattered throughout the cities. In situ observations, including dense networks of meteorological measurements in urban environments and the associated land surface fluxes are available for a very small number of cities (e.g., Ando & Ueyama, 2017; Kotthaus & Grimmond, 2012; H. C. Ward et al., 2013) and even in those they are localized. An alternative is offered by satellite retrievals of the earth's surface temperature, which have provided fine resolution data for decades now (e.g., Wan, 2008), allowing global scale

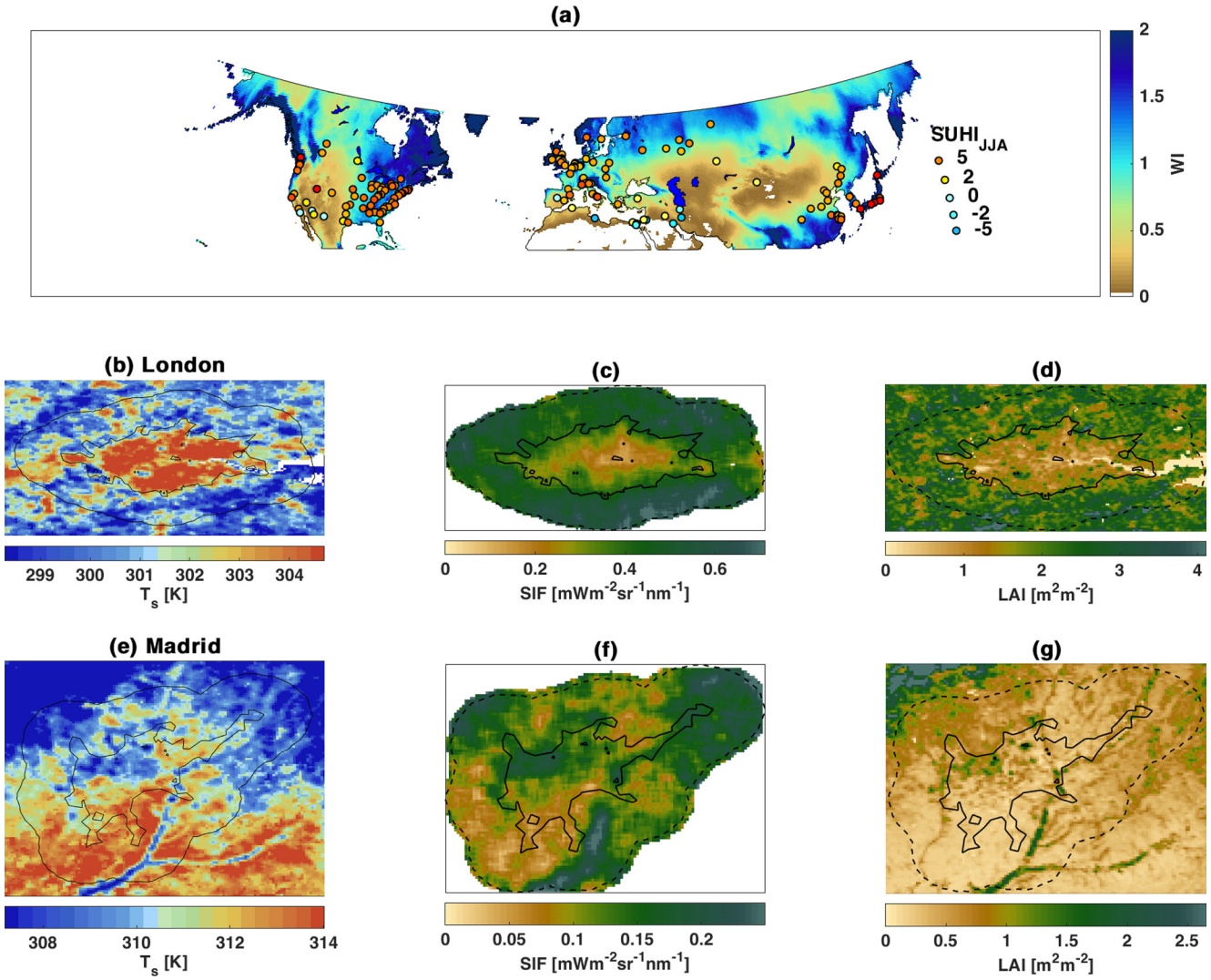

Figure 1. (a) Locations of the city clusters analyzed. Background colors correspond to the Wetness Index (WI) and marker colors to the average summertime intensity of SUHIs during day. (b–d) Maps of the average surface daytime temperature, SIF and LAI during summer (JJA) for London. Solid lines show the boundaries of the city clusters and dashed lines the boundaries of the rural surrounding. (e–g) Same for Madrid.

SUHI estimations (e.g., Chakraborty & Lee, 2019; Clinton & Gong, 2013). However, only recently, additional satellite derived data have become available at very high spatial resolutions, including leaf area (Garrigues et al., 2008), plant photosynthetic rates (Köhler et al., 2018), land use (Buchhorn et al., 2020), and building characteristics (Li, Koks, et al., 2020). These observations provide an unprecedented opportunity to quantify all relevant factors controlling SUHIs in detail, including the typology and function of urban vegetation.

In this study, we combine multiple current-generation remote sensing data, to identify global patterns of urban green cover, evaporative cooling, and SUHIs.

2. Data and Methods

2.1. Data

Publicly available data were used in this study.

2.1.1. Properties of the Built Environment

City clusters for the Northern Hemisphere were obtained by Wang et al. (2019). In this study, the 145 largest urban clusters in terms of extent were used (Figure 1a). For each urban cluster we defined a surrounding area with a width of 0.1° (~10 km) outside the cluster's boundary as a reference "rural" area.

The fraction of man-made impervious surfaces at a 30 m resolution was derived from Landsat images (Brown de Colstoun et al., 2017). Average building heights for each cluster were estimated using a recently published data set (Li, Koks, et al., 2020). The data set includes all of Europe, North America and China, and the statistical analysis that involves building heights focuses on a subset of 112 city clusters, excluding those located in North Africa and Asia, except China. Population data for all city clusters were obtained from Jones and O'Neill (2016). The 10-day average black and white sky broadband albedos were retrieved by SPOT-VGT, available at the Copernicus Data Center.

2.1.2. Surface Temperature and Climate

Monthly averages of day and night SUHI intensities were estimated using the land surface temperature difference of the built-up pixels within the urban clusters and the nonbuilt-up pixels of their surrounding areas, as estimated by MODIS, using the daily scenes from AQUA and TERRA satellites for 2018–2019 (spatial resolution of 1 km). The built-up and nonbuilt-up pixels were based on the European Space Agency's Climate Change Initiative Land Cover data set for 2018 at 300 m resolution (Bontemps et al., 2013). Global estimates of the wetness index, defined as the ratio of annual precipitation over annual potential evapotranspiration, were obtained using the CRU v4.02 data set (Harris et al., 2020) at a 0.5° resolution.

2.1.3. Urban Green Infrastructure

Vegetation properties and its activity within cities were also quantified. Vegetation properties included vegetation type and Leaf area index (LAI). LAI at 1 km spatial resolution for 2018 and 2019 were retrieved by SPOT-VGT. The fractions of trees, crops, shrubs, bare land, mosses and areas of permanent water cover, at 100m resolution for 2015 were obtained by the Copernicus Global Land Service (Buchhorn et al., 2019). Vegetation activity was quantified using Solar Induced Fluorescence (SIF) retrievals at 740 nm from the sensor on board the Copernicus Sentinel-5 Precursor satellite, as part of the TROPOMI mission (Köhler et al., 2018). The instrument has a swath width of ~2600 km allowing for the first time SIF retrievals at fine spatial scales (~7×3.5 km^2) at daily resolution. The satellite was launched in October 2017 and has been collecting data since then. The full record for 2018 and 2019 ungridded SIF retrievals was employed here, using the bias correction proposed by Köhler et al. (2018). SIF is a proxy for the photosynthetic activity of terrestrial ecosystems and is directly linked to transpiration and carbon assimilation by vegetation (e.g., Köhler et al., 2018).

2.2. Methods

For each urban cluster and its corresponding surrounding area, we calculated the average monthly SIF, LAI, (black and white sky) albedo (α) and day/night surface temperatures. Day ($SUHI_d$) and night ($SUHI_d$) SUHIs were estimated using the descending and ascending orbit retrievals of the TERRA (and AQUA) satellite, respectively. The metrics used to describe the land cover of each area were the average pervious land fraction, that is areas without man-made structures or permanent water, and the fractions of vegetated land covered by trees, crops, and low stature vegetation (grass and shrub). Vegetation phenology in both urban and rural areas was defined through the start (SOS) and end (EOS) of season dates. As SOS we defined the first crossing within the year when the 20 day rolling average of SIF time series exceeds 20% of its annual maximum value. EOS was defined as the date of the last crossing. Finally, for each city cluster, we estimated the average building height (H), wetness index (WI), that is the ratio of average annual precipitation and potential ET ($WI = P/PET$), and its population density (P_d). Note that the analyses here are performed considering all variables as city-scale averages. This inevitably reduces the heterogeneity of urban properties to their first statistical moments (i.e., mean and variance) but allows a systematic comparison of urban areas, their climate and vegetation characteristics (see discussion in Manoli, Fatich, Schläpfer, et al., 2020).

The statistical correlation between variables was established through the Pearson correlation coefficient and statistical significance was estimated based on p-values. The relative importance of each variable in

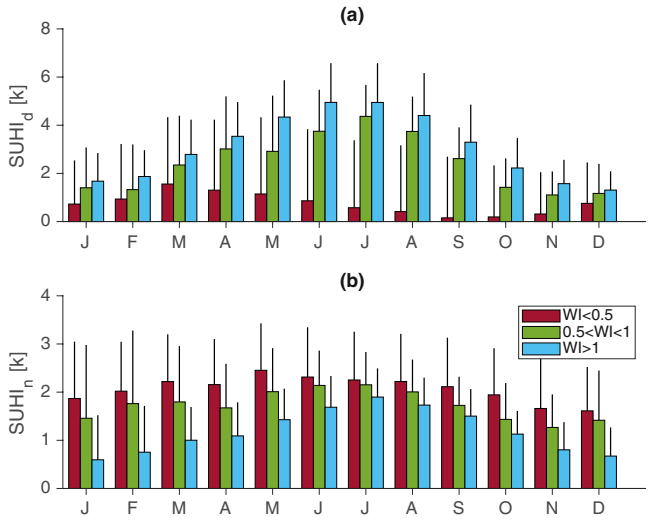

Figure 2. (a) Seasonal patterns of $SUHI_d$ intensities for dry (red), intermediate (green), and wet (blue) cities. Bar heights represent the average value of monthly $SUHI_d$ for all sites within the Wetness Index (WI) limits: dry WI < 0.5, intermediate 0.5 < WI < 1, wet WI > 1. Bars correspond to one standard deviation. (b) Same for $SUHI_n$.

explaining SUHIs was estimated using the partial least squares (PLS) regression, and their corresponding VIP (variable importance in projection) scores. Each variable was standardized by its standard deviation before performing the PLS regression. In the presented results, the four first principle components were used. Common linear and nonlinear (exponential in this study) regression analyses were also performed between variables using ordinary least squares, and statistical significance was assessed using the corresponding p-values. All data analysis was carried out in MATLAB R2020a.

3. Results and Discussion

3.1. The Dominant Role of Evaporative Cooling

Both $SUHI_d$ and $SUHI_n$ in the northern hemisphere have distinct seasonal patterns that change with the wetness index of the background climate (Figure 2). $SUHI_d$ in wet areas (WI > 1) peaks during summer season (June to August) with intensities $SUHI_d = 4.76 \pm 1.7$ K (Figure 2a). $SUHI_d$ in arid and semi-arid areas (WI < 0.5) are on average lower than wet cities throughout the whole year, and peak in early spring with intensities up to $SUHI_d = 1.56 \pm 2.8$ K during March. $SUHI_n$ is on average lower than $SUHI_d$ ($\overline{SUHI_n} = 1.5$ K, $\overline{SUHI_d} = 2.4$ K) throughout the year. $SUHI_n$ lacks a seasonal pattern in wet areas, whereas in arid and semi-arid places a clear seasonal pattern exists, with a peak during summer ($SUHI_n = 2.26 \pm 1.0$ K, for sites with a WI < 0.5), approximately 4 months later than the respective $SUHI_d$ (Figure 2b).

Similar results regarding the seasonal pattern of both $SUHI_d$ and $SUHI_n$ and their dependence on background climate have been previously documented for a number of cities (e.g., Manol, Fatichi, Bou-Zeid, & Katul, 2020; Schwarz et al., 2011; Zhou et al., 2014), confirming the robustness of this behavior. The differences between $SUHI_d$ and $SUHI_n$ rely on the different processes that operate during day and night. While $SUHI_n$ depend mostly on "abiotic" factors, such as the thermal capacity of urban/rural surfaces, anthropogenic heat emissions, and the intensity of boundary layer atmospheric turbulence (T. R. Oke, 1995), $SUHI_d$ depends also on "biotic" factors, and plant activity in particular. Plants transpire during day, altering the land surface energy budget by lowering the Bowen ratio, and thus lowering the temperature of vegetated areas relative to the impervious surfaces of cities.

Using two cities as examples of a wet (London) and relatively dry (Madrid) climate, we can gain further insights into the role of vegetation activity and how the seasonal patterns of $SUHI_d$ change with background climate wetness (Figure 3). The seasonal pattern of $SUHI_d$ is clearly linked with transpiration (i.e., evaporative cooling) since vegetated areas exhibit the lowest surface temperatures (Figures 1b–1g). This is also reflected in the difference in vegetation properties. In London, the maximum differences between urban and rural δLAI, and δ SIF occur during summer, when the highest $SUHI_d$ also occurs. Both LAI and SIF are approximately −35% (Figures 3a and 3b) lower during summer inside the city. In Madrid, the largest values of δLAI and δSIF also occur when $SUHI_d$ peaks, but in such a drier climate this happens during spring and the magnitude of difference is significantly lower (∼−10% (Figures 3a and 3b). As the seasonal patterns of δLAI and δSIF are identical to $SUHI_d$, and their magnitudes scale proportionately (Figure 3c), this is a strong indication of the importance of the evaporative cooling effect by plant photosynthesis and transpiration, on the daytime SUHIs (as statistically quantified in the following). However, whether evaporative cooling is the dominant control of $SUHI_d$ is still an open question. Recent studies, primarily based on models, suggest that urban-rural changes in evapotranspiration are the key drivers of urban warming (e.g., D. Li et al., 2019; Manoli et al., 2019), but there is also evidence that $SUHI_d$ intensities are strongly modulated by urban-rural differences in convective heat dissipation in humid and dry climate (e.g., Grimmond & Oke, 1999; Li, Bou-Zeid, et al., 2020; Zhao et al., 2014).

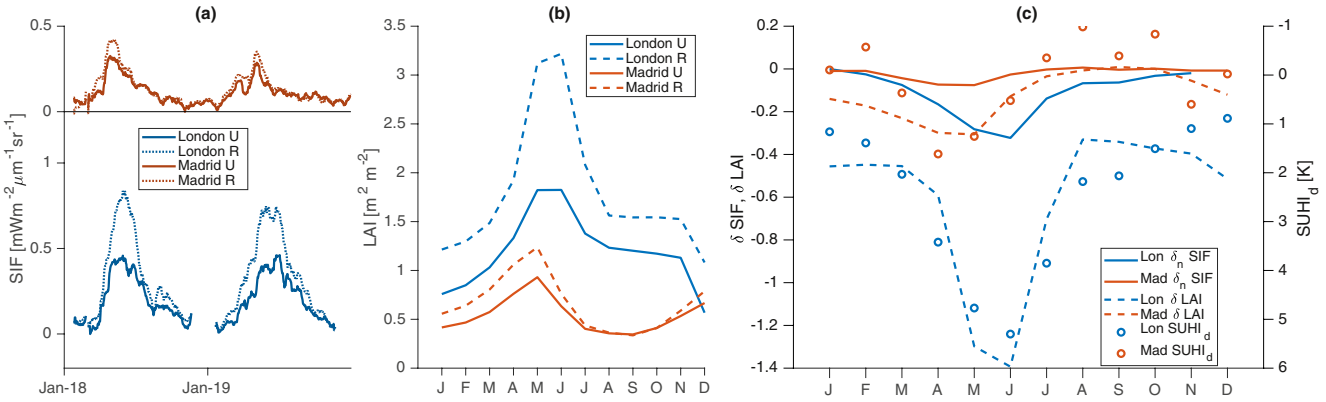

Figure 3. (a) Time series of daily SIF retrievals for Madrid (orange) and London (blue). Solid lines correspond to the urban cluster and dashed lines to rural surroundings. All time series are 10-day rolling averages. (b) Monthly average values of LAI for London (blue) and Madrid (orange). Solid lines correspond to the urban cluster and dashed lines to rural surroundings. (c) Monthly average values of δLAI (dashed lines), δSIF (solid lines) and SUHI$_d$ (circles), for London (blue) and Madrid (orange).

In order to quantify the relative importance of transpirative cooling in comparison to the remaining factors controlling the intensity of SUHIs, we performed a correlation analysis and a PLS regression between the intensities of SUHI$_d$ and SUHI$_n$, biotic factors controlling transpiration (SIF, LAI), and abiotic factors related to the urban fabric (building height: H, built area fraction: UC, albedo; α), background climate (WI), and population density (P_d), as a proxy for anthropogenic heat emissions (Figure 4). As expected SUHI$_n$ does not depend significantly on any biotic factor, given the absence of plant photosynthesis during night, and it is rather dependent on the urban form (Figure 4b). Specifically, SUHI$_n$ increases with the built fraction and decreases with building height (Figure 4a). A higher fraction of built area is related to higher heat storage capacity of buildings and streets, absorbing more heat during day and releasing it during night. Higher building heights, increase the urban roughness, favoring heat convection from the land to the atmosphere, and thus reducing surface temperatures. However, the robustness of this result is not strong, as the correlation between SUHI$_n$ and H is $r = -0.16$, (p-value = 0.09). Both, the fraction of built areas and building heights are correlated with population density (Figure S1), which could partially reflect the impact of anthropogenic heat emissions.

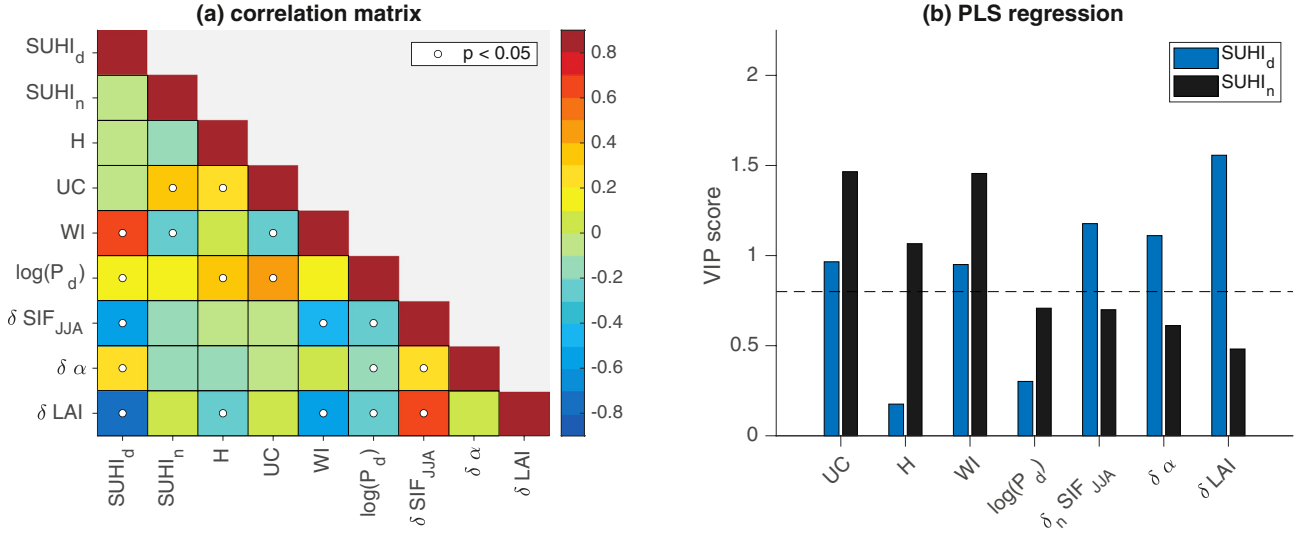

Figure 4. (a) Correlation matrix between all variables considered in this study. Colors correspond to the values of the Pearson correlation and circles indicate statistical significance. (b) Variable Importance in Projection (VIP) according to a partial least squares (PLS) regression, explaining the variability of SUHI$_d$ (blue) and SUHI$_n$ (black). Variables with a VIP < 0.8 (dashed line) are statistically considered as not influential. δ indicates urban minus rural differences of the analyzed variables.

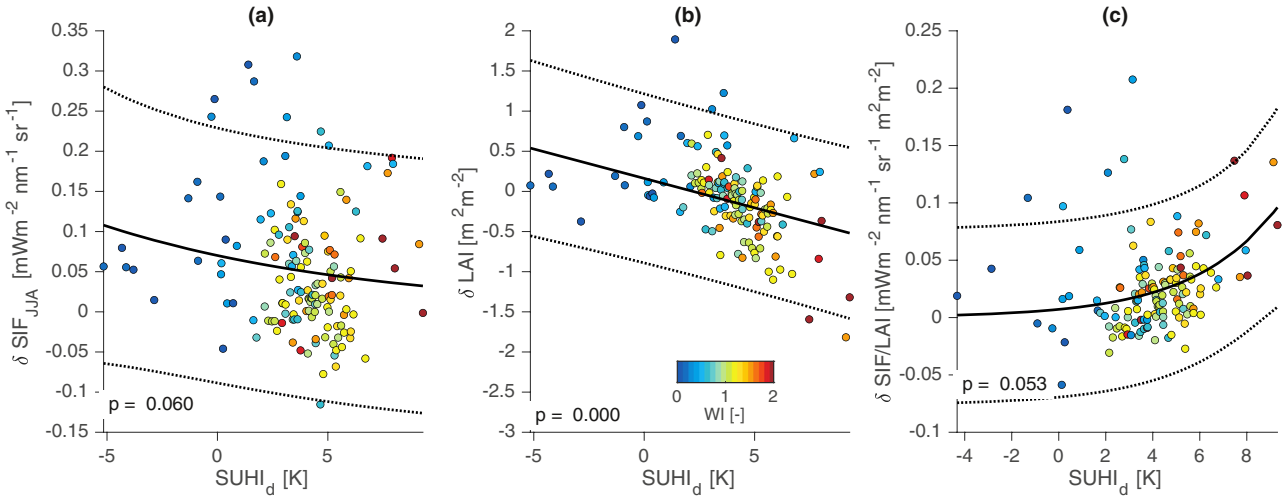

Figure 5. Scatterplot between summertime (JJA) average values of $SUHI_d$ and δSIF (a), δLAI (b) and δSIF/LAI (c). Solid lines correspond to a fitted exponential (a and c) or linear (b) model and dashed lines to its uncertainty bounds. Maker colors correspond to the WI of each site. LAI, Leaf area index; SIF, Solar Induced Fluorescence.

Contrary, $SUHI_d$ is significantly affected by transpirative cooling. In fact, the differences of both LAI and SIF between the urban and rural environment explain the largest fraction of the variability of $SUHI_d$, with LAI being the single most influential variable (Figure 4b). The difference between urban and rural albedos, modifying the amounts of net radiation on the land surface, also play a significant role, but with a lower importance than transpiration (reflected in LAI and SIF, Figure 4b). As expected, δLAI and δSIF (i.e., the difference between urban and rural) are negatively correlated with $SUHI_d$, highlighting that increasing LAI and SIF inside the cities contribute to evaporative cooling. $\delta\alpha$ is weakly but positively correlated with $SUHI_d$. This counter-intuitive correlation (i.e., cities with higher albedos having stronger $SUHI_d$) is related to the fact that typically a lack of green spaces in cities coincides with higher albedos (i.e., man-made structures have a higher albedo than vegetation) (Figure S1). Population density, even though positively correlated with building heights and the fraction of built area, is not significantly affecting $SUHI_d$ intensities. Overall, this extensive data set clearly points to an extremely dominant role of transpiration (i.e., evaporative cooling) for the magnitude of $SUHI_d$, in agreement with (e.g., Clinton & Gong, 2013; Kumar et al., 2017; Peng et al., 2012), and the importance of the urban fabric (i.e., man-mad structures) for the magnitude of $SUHI_n$ (e.g., Li, Schubert, et al., 2020; Sobstyl et al., 2018).

3.2. The Importance of Urban Green Spaces and Plant Type Composition

Given the major association between urban-rural changes in evapotranspiration and the magnitude of $SUHI_d$, and the rising interest in urban vegetation as heat mitigation measure, it is crucial to understand how vegetation structure and plant physiology depend on background climate, and how they impact the intensity of $SUHI_d$. δSIF is significantly affected by both $SUHI_d$ (Figure 5a) and WI (Figure S1). The reductions in SIF within the urban environment are highest for the wettest sites. In sharp contrast, for hyper-arid sites, SIF was found to be higher within the urban clusters than its surrounding rural areas. With higher SIF reductions occurring in the wettest sites, higher $SUHI_d$ intensities were observed in these cities (Figure 5a). Total SIF is a proxy of total photosynthetic rate and it depends on the leaf scale photosynthesis, representative of plant physiological responses to environmental forcing, and on the total available leaf area. To disentangle those two factors, we analyzed the behavior of LAI and the scaled quantity SIF/LAI as a proxy of plant physiological responses per unit of leaf area. LAI and SIF have an identical dependence structure with $SUHI_d$ and WI (Figure 5b). However, the statistical dependence between LAI reductions and both WI and $SUHI_d$ was significantly higher than for SIF. In other words, plant biophysical effects are more relevant than physiological effects. SIF/LAI was on average higher inside the cities with an increasing tendency with $SUHI_d$ intensities (Figure 5c). This increase primarily occurred at the wettest sites. Given that the wettest sites are predominately located in colder climates, vegetation is likely benefiting from increased temperature inside

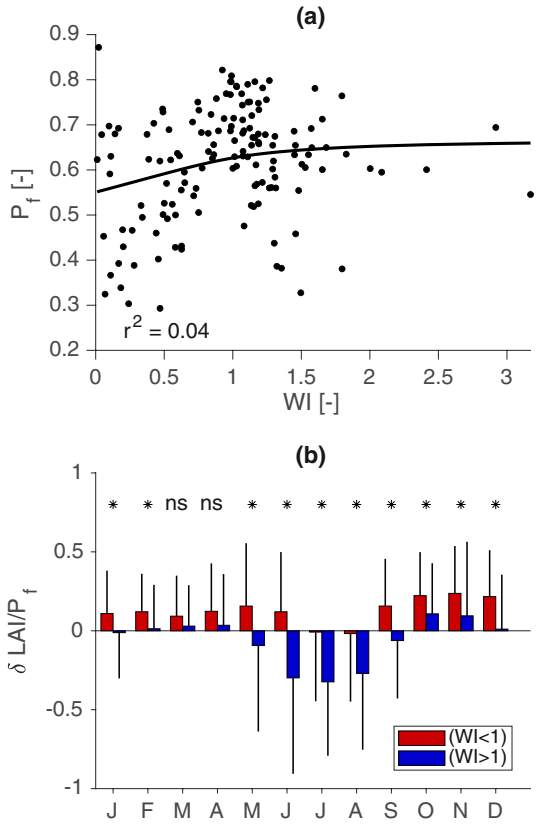

Figure 6. (a) Scatterplot between Wetness Index (WI) and the fraction of permeable space within cities (P_f). (b) Monthly errorbars of the difference between LAI/P_f (δLAI/P_f) inside and outside the cities. Bars show the mean values and line widths one standard deviation. Blue (red) bars correspond to wet (dry) sites. Asterisks show the months for which the distribution of δLAI/P_f is statistically significantly different between dry and wet sites based on a Welch test at a 5% confidence. "ns" stands for not significant differences.

the city, which raises photosynthetic rates. However the dependence of SIF/LAI to $SUHI_d$ is not statistically significant ($p > 0.05$). Additional factors that can contribute to the overall higher SIF/LAI values for all climates can be attributed to enhanced nitrogen deposition within cities, their elevated atmospheric CO_2 concentrations (e.g., Gregg et al., 2003), common irrigation and fertilization practices [e.g., Manol, Fatichi, Bou-Zeid, & Katul, 2020], and increased levels of available light [e.g., Bennie et al., 2016].

Given that plant physiological changes in urban clusters and their surroundings are weakly dependent on either WI or $SUHI_d$, δLAI explains most of the dependence of SIF and thus evaporative cooling on WI and $SUHI_d$. Potential candidate variables that can explain the dependence of δLAI to WI are the availability of green space and LAI per unit of green space. We found an increase in green space availability with background climate (Figure 6a) but the relation is very weak ($r^2 = 0.04$), and thus cannot explain the dependence of δLAI on WI. In contrast, LAI for unit of urban pervious (nonbuilt) areas (LAI/P_f) has a clear dependence on background climate (Figure 6b). Differences in LAI/P_f are highest during summer. In wet climates (WI > 1), LAI/P_f is significantly higher in the surrounding rural areas during summer than within city clusters (Figure 6b) while in dry climates (WI < 1) there is not a statistically significant difference between LAI/P_f inside and outside cities during the growing season (Figure 6b). Is spring and fall, in dry areas, LAI/P_f is higher inside than outside the cities. We can thus conclude that the available leaf area, and LAI/P_f in particular, rather than plant physiological responses to microclimate explain the dependence structure between δSIF, WI, and $SUHI_d$ during the warmest months.

Differences in LAI/P_f (i.e., the leaf area per unit green space) between urban and rural areas can be caused by either plant phenology or species composition. In agreement with previous studies, the average growing season length was found to be longer in cities (e.g., Wang et al., 2019; X. Zhang et al., 2004) by 7.7 $\pm$ 23.5 days. The start of the growing season occurs 1.14 $\pm$ 15.8 days earlier (Figure 7a) and is independent of background climate. The end of season occurs 8.8 $\pm$ 18.5 days later inside cities (Figure 7b). There is a negative correlation (Figure 7b), between the delay of the end of season date and background climate, with cities in dry climates sustaining active vegetation for longer. As drier cities in our analysis are located in warm semi-arid and arid climates, the delay of the EOS data is unlikely to be related to temperature increases inside the city, and it is most likely related to either continuous irrigation provided to plants, allowing them to sustain a prolonged period of activity or as Wang et al. (2019) proposed, due to elevated CO_2 concentrations in cities, leading to water savings in the root zone (Fatichi et al., 2016), due to reduced stomatal conductance with higher CO_2 (e.g., Paschalis et al., 2017). However the difference in the length of the vegetation active season is not significantly correlated ($p > 0.05$) with the differences in LAI/P_f and thus cannot explain dependence of $SUHI_d$ on WI.

In contrast, there is also a strong dependence between background climate and the difference in land cover in pervious spaces inside and outside cities, and in particular vegetation composition (Figure 7d; Figure S2). In agreement with the well-known global distribution of trees (e.g., Hirota et al., 2011), the fraction of forest cover f increases with increasing wetness. This occurs in both urban and rural areas. However, vegetation in wet cities contains on average a larger fraction of low stature vegetation (shrubs, grasses, and crops) compared to its surrounding rural area, which typically consist of native forests. In dry locations, the fraction of green spaces with trees is similar between the urban and rural areas, and it is in general low. On average, the green spaces of dry cities consist to a larger degree of grasses and shrubs (e.g., parks and gardens) at the expenses of lower crop fractions (Figure S2). The difference in tree cover fraction (or the complementary

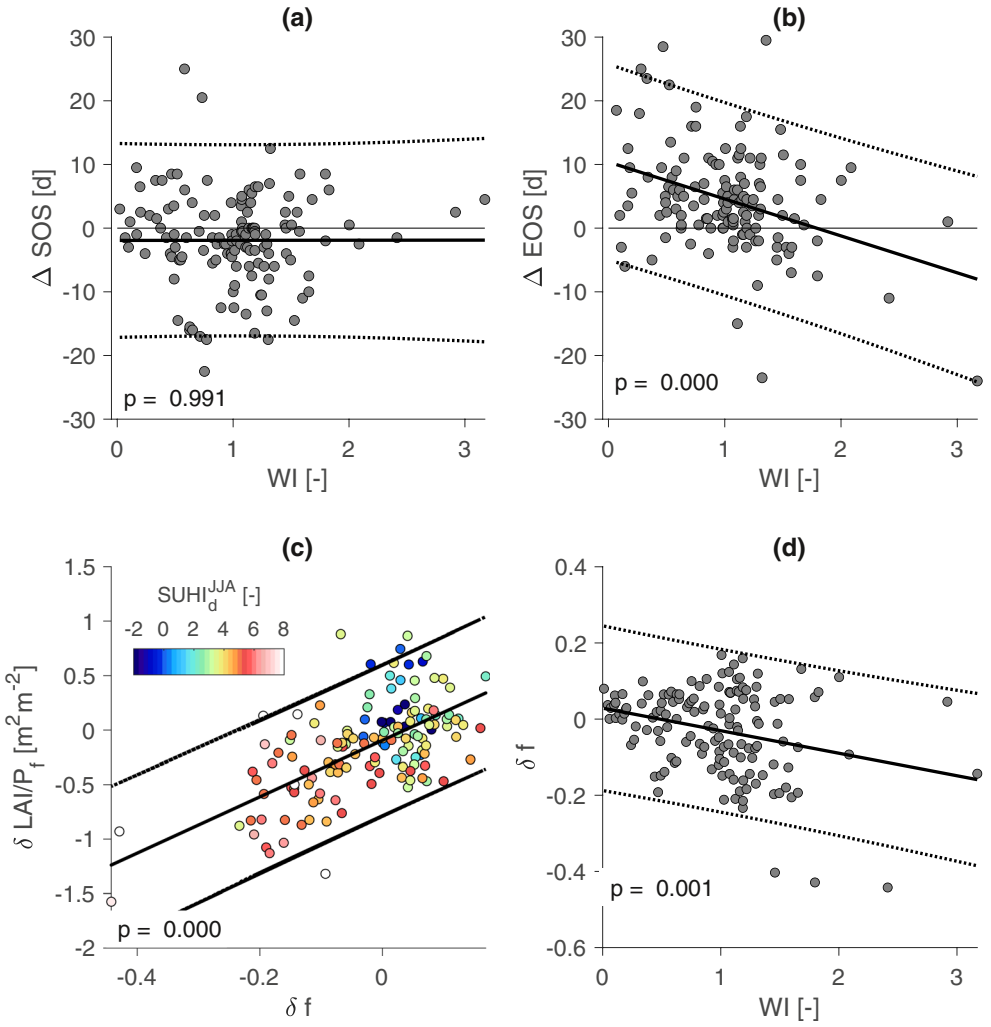

Figure 7. Scatterplots between Wetness Index (WI) and ΔEOS (a) and ΔSOS (b) for all city clusters. Solid lines correspond to a fitted linear model and dashed lines to its uncertainty bounds. (c) Scatterplot between δf and $\delta LAI/P_f$, where f is the tree cover fraction of pervious surfaces. Marker colors show the value of $SUHI_d$ during summer for each city. (d) Scatterplot between WI and δf. Solid lines correspond to a fitted linear model and dashed lines to its uncertainty bounds.

differences in low stature vegetation fractions) between cities and their surroundings (δf) can explain $\delta LAI/Pf$ to a large extent (Figures 7c, Figure S2). δf is also statistically significantly dependent of WI, while the respective differences of crop and grass cover distributions are not as strongly dependent on WI (Figure S2). In summary, on average, in wet areas, δf is low, causing a large reduction of $\delta LAI/Pf$, and subsequently SIF, and transpiration cooling. Integrating all these information, we can conclude that the key attribute that determines the strength of $SUHI_d$ is not only the amount of urban green spaces (or nonbuilt surfaces) but the type of vegetation that compose them.

3.3. Implications for Green Infrastructure Design

LAI as a metric for sustainable urban development has been proposed previously in architectural design (Ong, 2003). In this study, we clearly illustrate that the major factor affecting the difference between urban and rural LAI, and its implications for the developments of SUHIs, are primarily related to changes in the fraction of high stature vegetation (e.g., urban forests). In other words, urban greenery consists more often of mowed lawns and scattered trees, which cannot replicate the LAI density of rural counterparts in wet regions. Maintenance and expansion of urban forests rather than generic urban greening, is thus found to

be a key factor for mitigating SUHIs and, more broadly, improve urban microclimate. Strategic growing of urban forests is also a widely accepted solution for improving ecosystem services, human well-being, and enhancing biodiversity (Endreny, 2018). However, both maintenance and expansion of urban forests is a major challenge. High stature vegetation requires water that might not be available in dry places, where water scarcity is often a major issue of concern. Large amounts of irrigation are needed to sustain non-native urban green forests, which conflicts with sustainable water management practices (e.g., L. Liu and Jensen, 2018). Regions currently considered wet, could also experience longer dry periods in the future (e.g., Feng et al., 2013; Fu et al., 2013), with a simultaneous increase in atmospheric drought and plant water stress, that could only be alleviated with extensive irrigation (e.g., Ukkola et al., 2020). In addition, expansion and retrofitting of urban forests in already densely populated cities is a major challenge because of high costs and limited space availability. A sustainable urban design alternative that could partially alleviate both the need for extensive irrigation and engineering works, is the maintenance of "urban reserves" by integrating remainders of natural vegetation within the urban form. Native vegetation adapted to its local climate can be sustained and remain active, and thus provide evaporative cooling, without the need of providing copious amounts of water (e.g., Paschalis et al., 2018).

The strong dependence of our results on urban green cover and background climate, also highlights the need for appropriate models to design optimal vegetation strategies for cities. In order to properly quantify the land surface energy budget, we should take into account urban vegetation, its dynamics (e.g., LAI temporal and spatial dynamics), and its responses to both climate and anthropogenic interventions (e.g., irrigation). Detailed models that integrate all essential physical, hydrological, and plant physiological processes in the urban environment have only recently been introduced (e.g., Meili et al., 2020; Nice et al., 2018) and their incremental use could lead to a better and sustainable design of urban landscapes from a microclimatic perspective.

3.4. Limitations and Future Directions

There is undoubtedly a need for detailed, spatially distributed, observations of urban bio-climatic conditions. In this study, we focused on SUHIs, that can be estimated via remote sensing globally. SUHIs, even though in the long term strongly correlated with CUHI, cannot provide detailed information concerning thermal comfort and the impact of heat stress to human health (e.g., Martilli et al., 2020). For instance, in addition to the high uncertainty in remotely sensed surface temperature over urban areas due to thermal anisotropy (Hu et al., 2016), satellites may overestimate the "true" SUHI by primarily capturing the higher temperatures of roof tops. For more accurate estimation of urban heat stress and to better validate modeling and remote sensing products, in-situ dense monitoring networks of temperature, wind, humidity, and radiation at the pedestrian scale, currently not available in most cities, are essential. Beyond meteorological data obtained by weather services within cities, citizen science data that are now being collected can provide complementary, high resolution information in space and time (e.g., Chapman et al., 2017). Temperature satellite remote sensing data that were used in this study have a moderate resolution and were obtained by sun-synchronous sensors, which cannot describe in detail the diurnal variability of land surface temperature. Data fusion from multiple high resolution satellites and geostationary satellite data, typically with coarser resolution, can in the future further strengthen our results.

Monitoring urban heat fluxes and the performance of urban vegetation is also crucial. In this study, we relied exclusively on remote sensing data to assess the productivity and structure of urban vegetation. However, remote sensing measurements can be noisy and occasionally unreliable. SIF retrievals for example are contaminated by cloud cover, background reflectivities of the urban environment (e.g., Zeng et al., 2019) and can be impacted by vegetation structure itself (Dechant et al., 2020). Also SIF retrievals, to this day, have spatial scales that cannot resolve the fine urban landscape heterogeneity. Complementary measurements, such as regular campaigns of leaf gas exchange measurements, urban eddy covariance systems, soil moisture and sapflux monitoring in experimental plots within cities would provide crucial complimentary fine-scale information regarding plant functioning. Additionally, as multi- and hyper-spectral sensors can now be transported by low cost Unmanned Aerial Vehicles (UAVs), frequent low altitude monitoring campaigns can provide essential data to constrain plant photosynthetic rates, canopy structural properties, and even leaf stoichiometry (e.g., Bandopadhyay et al., 2020; H. Liu et al., 2017; Mathews & Jensen, 2013).

Finally, as new streams of data become available, advanced statistical techniques, such as machine learning, can also provide the necessary methodological tools to explore synergies between multiple sources of spatial information. Some of these advanced machine learning tools can have improved prediction accuracy compared to classical statistical frameworks, but may also introduce more obstacles for clear mechanistic interpretations.

4. Conclusions

In this study, we exploited the potential of state-of-the-art remote sensing data to provide a mechanistic understanding of vegetation-climate interactions in complex urban settings and to quantify the links between urban fabric, green spaces, vegetation types, and SUHIs. Night-time SUHIs ($SUHI_n$) are on average smaller than their corresponding day-time SUHIs ($SUHI_d$) and depend predominantly on the urban fabric (building heights, building density). $SUHI_d$ are strongly correlated with background climate (as defined by the wetness index WI), and possess a distinct seasonal pattern that peaks during summer in wet areas and early spring in seasonally dry areas. A major factor for the development of strong summertime SUHIs in wet places is the reduction of evaporative cooling in cities. This reduction is due to the difference in LAI between cities and their surroundings, and largely independent from plant physiological and phenological behavior. Change in LAI and its dependence on WI is associated with a difference in vegetation type between urban and rural areas. In particular, a reduction in the fraction of forested areas in cities, leads to a strong decrease in LAI and a weaker evaporative cooling. Therefore, our results highlight the importance of preserving urban forests as natural reserves, rather than simply "greening" cities for reducing the daytime SUHI effect.

Conflict of Interest

The authors declare no conflicts of interest relevant to this study.

Data Availability Statement

- MODIS Land Surface Temperature (https://modis.gsfc.nasa.gov/data/dataprod/mod11.php)
- TROPOMI SIF data (ftp://fluo.gps.caltech.edu/data/tropomi/)
- Impermeable fraction (https://sedac.ciesin.columbia.edu/data/set/ulandsat-gmis-v1/data-download)
- Building height (https://landbigdata.github.io/cscproject/)
- Albedo (https://land.copernicus.eu/global/products/sa)
- LAI (https://land.copernicus.eu/global/products/lai)
- Vegetation cover fraction (https://land.copernicus.eu/global/products/lc)
- City Clusters (https://drive.google.com/drive/folders/1yzcoRAjjubiLDqlg6zbLUCfE_m1mHAsL?usp=sharing)
- Population (https://sedac.ciesin.columbia.edu/data/set/gpw-v4-population-count-rev11/maps)
- CRU data (https://crudata.uea.ac.uk/cru/data/hrg/).

Acknowledgments
A. Paschalis acknowledges financial support from NERC (NE/S003495/1). G. Manoli was supported by the "The Branco Weiss Fellowship - Society in Science" administered by ETH Zurich. S. Fatichi would like to thank the support of the Singapore Ministry of Education Academic Research Fund Tier 1 through the project "Bridging scales from below: The role of heterogeneities in the global water and carbon budgets. N. Meili conducted research at the Future Cities Laboratory at the Singapore-ETH Centre, which was established collaboratively between ETH Zurich and Singapore's National Research Foundation (FI370074016) under its Campus for Research Excellence and Technological Enterprise programme.

References

Allen, L., Lindberg, F., & Grimmond, C. S. B. (2011). Global to city scale urban anthropogenic heat flux: Model and variability. *International Journal of Climatology*, *31*(13), 1990–2005. https://doi.org/10.1002/joc.2210

Ando, T., & Ueyama, M. (2017). Surface energy exchange in a dense urban built-up area based on two-year eddy covariance measurements in Sakai, Japan. *Urban Climate*, *19*, 155–169. https://doi.org/10.1016/j.uclim.2017.01.005

Angel, S., Parent, J., Civco, D. L., Blei, A., & Potere, D. (2011). The dimensions of global urban expansion: Estimates and projections for all countries, 2000-2050. *Progress in Planning*, *75*(2), 53–107.

Arnfield, A. J. (2003). Two decades of urban climate research: A review of turbulence, exchanges of energy and water, and the urban heat island. *International Journal of Climatology*, *23*(1), 1–26. https://doi.org/10.1002/joc.859

Avolio, M. L., Pataki, D. E., Trammell, T. L. E., & Endter-Wada, J. (2018). Biodiverse cities: The nursery industry, homeowners, and neighborhood differences drive urban tree composition. *Ecological Monographs*, *88*(2), 259–276. https://doi.org/10.1002/ecm.1290

Bandopadhyay, S., Rastogi, A., & Juszczak, R. (2020). Review of top-of-canopy sun-induced fluorescence (SIF) studies from ground, UAV, airborne to spaceborne observations. *Sensors*, *20*(4), 1144. https://doi.org/10.3390/s20041144

Bennie, J., Davies, T. W., Cruse, D., & Gaston, K. J. (2016). Ecological effects of artificial light at night on wild plants. *Journal of Ecology*, *104*(3), 611–620. https://doi.org/10.1111/1365-2745.12551

Bontemps, S., Defourny, P., Radoux, J., Van Bogaert, E., Lamarche, C., Achard, F., et al. (2013). Consistent global land cover maps for climate modelling communities: Current achievements of the ESA's land cover CCI. In *Proceedings of the ESA living planet symposium* (pp. 9–13). Edimburgh.

Brown de Colstoun, E., Huang, C., Wang, P., Tilton, J., Tan, B., Phillips, J., et al. (2017). Global man-made impervious surface (GMIS) dataset from landsat. Palisades, NY, USA. NASA Socioeconomic Data and Applications Center (SEDAC).

Buchhorn, M., Lesiv, M., Tsendbazar, N.-E., Herold, M., Bertels, L., & Smets, B. (2020). Copernicus global land cover layers-Collection 2. *Remote Sensing*, *12*(6), 1044. https://doi.org/10.3390/rs12061044

Buchhorn, M., Smets, B., Bertels, L., Lesiv, M., Tsendbazar, N., Herold, M., & Fritz, S. (2019). Copernicus global land service: Land cover 100m: Epoch 2015: Globe, Version V2. 0.2. Zenodo.

Chakraborty, T., Hsu, A., Manya, D., & Sheriff, G. (2020). A spatially explicit surface urban heat island database for the united states: Characterization, uncertainties, and possible applications. *ISPRS Journal of Photogrammetry and Remote Sensing*, *168*, 74–88. https://doi.org/10.1016/j.isprsjprs.2020.07.021

Chakraborty, T., & Lee, X. (2019). A simplified urban-extent algorithm to characterize surface urban heat islands on a global scale and examine vegetation control on their spatiotemporal variability. *International Journal of Applied Earth Observation and Geoinformation*, *74*, 269–280. https://doi.org/10.1016/j.jag.2018.09.015

Chakraborty, T., Sarangi, C., & Tripathi, S. N. (2017). Understanding diurnality and inter-seasonality of a sub-tropical urban heat island. *Boundary-Layer Meteorology*, *163*(2), 287–309. https://doi.org/10.1007/s10546-016-0223-0

Chapman, L., Bell, C., & Bell, S. (2017). Can the crowdsourcing data paradigm take atmospheric science to a new level? A case study of the urban heat island of London quantified using netatmo weather stations. *International Journal of Climatology*, *37*(9), 3597–3605. https://doi.org/10.1002/joc.4940

Chen, G., Li, X., Liu, X., Chen, Y., Liang, X., Leng, J., et al. (2020). Global projections of future urban land expansion under shared socioeconomic pathways. *Nature Communications*, *11*(1), 1–12. https://doi.org/10.1038/s41467-020-14386-x

Clinton, N., & Gong, P. (2013). Modis detected surface urban heat islands and sinks: Global locations and controls. *Remote Sensing of Environment*, *134*, 294–304. https://doi.org/10.1016/j.rse.2013.03.008

Dechant, B., Ryu, Y., Badgley, G., Zeng, Y., Berry, J. A., Zhang, Y., et al. (2020). Canopy structure explains the relationship between photosynthesis and sun-induced chlorophyll fluorescence in crops. *Remote Sensing of Environment*, *241*, 111733. https://doi.org/10.1016/j.rse.2020.111733

Endreny, T. A. (2018). Strategically growing the urban forest will improve our world. *Nature Communications*, *9*(1), 1160. https://doi.org/10.1038/s41467-018-03622-0

Fatichi, S., Leuzinger, S., Paschalis, A., Langley, J. A., Donnellan Barraclough, A., & Hovenden, M. J. (2016). Partitioning direct and indirect effects reveals the response of water-limited ecosystems to elevated CO2. *Proceedings of the National Academy of Sciences of the United States of America*, *113*(45), 12757–12762. https://doi.org/10.1073/pnas.1605036113

Feng, X., Porporato, A., & Rodriguez-Iturbe, I. (2013). Changes in rainfall seasonality in the tropics. *Nature Climate Change*, *3*(9), 811–815. https://doi.org/10.1038/nclimate1907

Fong, K. C., Hart, J. E., & James, P. (2018). A review of epidemiologic studies on greenness and health: Updated literature through 2017. *Current Environmental Health Reports*, *5*(1), 77–87. https://doi.org/10.1007/s40572-018-0179-y

Fu, R., Yin, L., Li, W., Arias, P. A., Dickinson, R. E., Huang, L., et al. (2013). Increased dry-season length over southern Amazonia in recent decades and its implication for future climate projection. *Proceedings of the National Academy of Sciences*, *110*(45), 18110–18115. https://doi.org/10.1073/pnas.1302584110

Garrigues, S., Lacaze, R., Baret, F., Morisette, J. T., Weiss, M., Nickeson, J. E., et al. (2008). Validation and intercomparison of global leaf area index products derived from remote sensing data. *Journal of Geophysical Research*, *113*, G02028 . https://doi.org/10.1029/2007jg000635

Gregg, J. W., Jones, C. G., & Dawson, T. E. (2003). Urbanization effects on tree growth in the vicinity of New York City. *Nature*, *424*(6945), 183–187. https://doi.org/10.1038/nature01728

Grimmond, C. S. B., Blackett, M., Best, M. J., Barlow, J., Baik, J.-J., Belcher, S. E., et al. (2010). The international urban energy balance models comparison project: First results from Phase 1. *Journal of applied meteorology and climatology*, *49*(6), 1268–1292. https://doi.org/10.1175/2010jamc2354.1

Grimmond, C. S. B., & Oke, T. R. (1999). Aerodynamic properties of urban areas derived from analysis of surface form. *Journal of Applied Meteorology*, *38*(9), 1262–1292. https://doi.org/10.1175/1520-0450(1999)038<1262:apouad>2.0.co;2

Gunawardena, K. R., Wells, M. J., & Kershaw, T. (2017). Utilising green and bluespace to mitigate urban heat island intensity. *Science of the Total Environment*, *584–585*, 1040–1055. https://doi.org/10.1016/j.scitotenv.2017.01.158

Harris, I., Osborn, T. J., Jones, P., & Lister, D. (2020). Version 4 of the CRU TS monthly high-resolution gridded multivariate climate dataset. *Scientific Data*, *7*(1), 1–18. https://doi.org/10.1038/s41597-020-0453-3

Heaviside, C., Vardoulakis, S., & Cai, X.-M. (2016). Attribution of mortality to the urban heat island during heatwaves in the West Midlands, UK. *Environmental Health*, *15*(1), 49–59. https://doi.org/10.1186/s12940-016-0100-9

Hirota, M., Holmgren, M., Van Nes, E. H., & Scheffer, M. (2011). Global resilience of tropical forest and savanna to critical transitions. *Science*, *334*(6053), 232–235. https://doi.org/10.1126/science.1210657

Howard, L., & Phillips, W. (1833). *The climate of London* (Vol. 1. International Association for Urban Climate(IAUC).

Hu, L., Monaghan, A., Voogt, J. A., & Barlage, M. (2016). A first satellite-based observational assessment of urban thermal anisotropy. *Remote Sensing of Environment*, *181*, 111–121. https://doi.org/10.1016/j.rse.2016.03.043

Jones, B., & O'Neill, B. C. (2016). Spatially explicit global population scenarios consistent with the shared socioeconomic pathways. *Environmental Research Letters*, *11*(8), 084003. https://doi.org/10.1088/1748-9326/11/8/084003

Köhler, P., Frankenberg, C., Magney, T. S., Guanter, L., Joiner, J., & Landgraf, J. (2018). Global retrievals of solar-induced chlorophyll fluorescence with tropomi: First results and intersensor comparison to OCO-2. *Geophysical Research Letters*, *45*, 10–456. https://doi.org/10.1029/2018gl079031

Kolokotroni, M., Ren, X., Davies, M., & Mavrogianni, A. (2012). London's urban heat island: Impact on current and future energy consumption in office buildings. *Energy and Buildings*, *47*, 302–311. https://doi.org/10.1016/j.enbuild.2011.12.019

Kotthaus, S., & Grimmond, C. S. B. (2012). Identification of Micro-Scale Anthropogenic CO2, heat and moisture sources - Processing eddy covariance fluxes for a dense urban environment. *Atmospheric Environment*, *57*, 301–316. https://doi.org/10.1016/j.atmosenv.2012.04.024

Kumar, R., Mishra, V., Buzan, J., Kumar, R., Shindell, D., & Huber, M. (2017). Dominant control of agriculture and irrigation on urban heat island in india. *Scientific Reports*, *7*(1), 1–10. https://doi.org/10.1038/s41598-017-14213-2

Li, D., & Bou-Zeid, E. (2013). Synergistic interactions between urban heat islands and heat waves: The impact in cities is larger than the sum of its parts. *Journal of Applied Meteorology and Climatology*, *52*(9), 2051–2064. https://doi.org/10.1175/jamc-d-13-02.1

Li, D., Liao, W., Rigden, A. J., Liu, X., Wang, D., Malyshev, S., & Shevliakova, E. (2019). Urban heat island: Aerodynamics or imperviousness? *Science Advances*, *5*(4), eaau4299. https://doi.org/10.1126/sciadv.aau4299
Li, M., Koks, E., Taubenböck, H., & van Vliet, J. (2020). Continental-scale mapping and analysis of 3-D building structure. *Remote Sensing of Environment*, *245*, 111859. https://doi.org/10.1016/j.rse.2020.111859
Li, Q., Bou-Zeid, E., Grimmond, S., Zilitinkevich, S., & Katul, G. (2020) Revisiting the relation between momentum and scalar roughness lengths of urban surfaces. *Quarterly Journal of the Royal Meteorological Society*, *146*, 3144–3164. https://doi.org/10.1002/qj.3839
Li, Y. Schubert, S., Kropp, J. P., & Rybski, D. (2020). On the influence of density and morphology on the urban heat island intensity. *Nature Communications*, *11*(1), 1–9. https://doi.org/10.1038/s41467-020-16461-9
Liu, H., Zhu, H., & Wang, P. (2017). Quantitative modelling for leaf nitrogen content of winter wheat using UAV-based hyperspectral data. *International Journal of Remote Sensing*, *38*(8–10), 2117–2134. https://doi.org/10.1080/01431161.2016.1253899
Liu, L., & Jensen, M. B. (2018). Green infrastructure for sustainable urban water management: Practices of five forerunner cities. *Cities*, *74*, 126–133. https://doi.org/10.1016/j.cities.2017.11.013
Manoli, G., Fatichi, S., Bou-Zeid, E., & Katul, G. G. (2020). Seasonal hysteresis of surface urban heat islands. *Proceedings of the National Academy of Sciences of the United States of America*, *117*(13), 7082–7089. https://doi.org/10.1073/pnas.1917554117
Manoli, G., Fatichi, S., Schläpfer, M., Yu, K., Crowther, T. W., Meili, N., et al. (2019). Magnitude of urban heat islands largely explained by climate and population. *Nature*, *573*(7772), 55–60. https://doi.org/10.1038/s41586-019-1512-9
Manoli, G., Fatichi, S., Schläpfer, M., Yu, K., Crowther, T. W., Meili, N., et al. (2020). Reply to Martilli et al.(2020): Summer average urban-rural surface temperature differences do not indicate the need for urban heat reduction. OSF Preprints.
Martilli, A., Krayenhoff, E. S., & Nazarian, N. (2020). Is the urban heat island intensity relevant for heat mitigation studies? *Urban Climate*, *31*, 100541. https://doi.org/10.1016/j.uclim.2019.100541
Mathews, A., & Jensen, J. (2013). Visualizing and quantifying vineyard canopy LAI using an unmanned aerial vehicle (UAV) collected high density structure from motion point cloud. *Remote Sensing*, *5*(5), 2164–2183. https://doi.org/10.3390/rs5052164
Meili, N., Manoli, G., Burlando, P., Bou–Zeid, E., Chow, W. T. L., Coutts, A. M., et al. (2020). An urban ecohydrological model to quantify the effect of vegetation on urban climate and hydrology (ut&c v1.0). Geoscientific Model Development.
Mills, G. (2014). Urban climatology: History, status and prospects. *Urban climate*, *10*, 479–489. https://doi.org/10.1016/j.uclim.2014.06.004
Murari, K. K., Ghosh, S., Patwardhan, A., Daly, E., & Salvi, K. (2015). Intensification of future severe heat waves in India and their effect on heat stress and mortality. *Regional Environmental Change*, *15*(4), 569–579. https://doi.org/10.1007/s10113-014-0660-6
Nice, K. A., Coutts, A. M., & Tapper, N. J. (2018). Development of the VTUF-3D v1.0 urban micro-climate model to support assessment of urban vegetation influences on human thermal comfort. *Urban climate*, *24*, 1052–1076. https://doi.org/10.1016/j.uclim.2017.12.008
Oke, T. (1982). The energetic basic of the urban heat island. *Quarterly Journal of the Royal Meteorological Society*, *108*(455), 1–24. https://doi.org/10.1256/smsqj.45501
Oke, T. R. (1995). The heat island of the urban boundary layer: Characteristics, causes and effects. In *Wind climate in cities* (pp. 81–107). Springer. https://doi.org/10.1007/978-94-017-3686-2_5
Oke, T. R., Mills, G., Christen, A., & Voogt, J. A. (2017). *Urban climates*. Cambridge University Press. https://doi.org/10.1017/9781139016476
Ong, B. L. (2003). Green plot ratio: An ecological measure for architecture and urban planning. *Landscape and Urban Planning*, *63*(4), 197–211. https://doi.org/10.1016/s0169-2046(02)00191-3
Pappas, C., Fatichi, S., & Burlando, P. (2016). Modeling terrestrial carbon and water dynamics across climatic gradients: Does plant trait diversity matter? *New Phytologist*, *209*(1), 137–151. https://doi.org/10.1111/nph.13590
Paschalis, A., Fatichi, S., Pappas, C., & Or, D. (2018). Covariation of vegetation and climate constrains present and future t/et variability. *Environmental Research Letters*, *13*(10), 104012. https://doi.org/10.1088/1748-9326/aae267
Paschalis, A., Katul, G. G., Fatichi, S., Palmroth, S., & Way, D. (2017). On the variability of the ecosystem response to elevated atmospheric CO2 across spatial and temporal scales at the duke forest face experiment. *Agricultural and Forest Meteorology*, *232*, 367–383. https://doi.org/10.1016/j.agrformet.2016.09.003
Peng, S., Piao, S., Ciais, P., Friedlingstein, P., Ottle, C., Bréon, F.-M., et al. (2012). Surface urban heat island across 419 global big cities. *Environmental Science & Technology*, *46*(2), 696–703. https://doi.org/10.1021/es2030438
Raymond, C., Matthews, T., & Horton, R. M. (2020). The emergence of heat and humidity too severe for human tolerance. *Science Advances*, *6*(19), eaaw1838. https://doi.org/10.1126/sciadv.aaw1838
Rotach, M. W. (1999). On the influence of the urban roughness sublayer on turbulence and dispersion. *Atmospheric Environment*, *33*(24–25), 4001–4008. https://doi.org/10.1016/s1352-2310(99)00141-7
Santamouris, M. (2014). On the energy impact of urban heat island and global warming on buildings. *Energy and Buildings*, *82*, 100–113. https://doi.org/10.1016/j.enbuild.2014.07.022
Schoetter, R., Cattiaux, J., & Douville, H. (2015). Changes of western european heat wave characteristics projected by the CMIP5 ensemble. *Climate Dynamics*, *45*(5–6), 1601–1616. https://doi.org/10.1007/s00382-014-2434-8
Schwarz, N., Lautenbach, S., & Seppelt, R. (2011). Exploring indicators for quantifying surface urban heat islands of European cities with MODIS land surface temperatures. *Remote Sensing of Environment*, *115*(12), 3175–3186. https://doi.org/10.1016/j.rse.2011.07.003
Seto, K. C., Fragkias, M., Güneralp, B., & Reilly, M. K. (2011). A meta-analysis of global urban land expansion. *PloS One*, *6*(8), e23777. https://doi.org/10.1371/journal.pone.0023777
Sobstyl, J., Emig, T., Qomi, M. A., Ulm, F.-J., & Pellenq, R.-M. (2018). Role of city texture in urban heat islands at nighttime. *Physical Review Letters*, *120*(10), 108701. https://doi.org/10.1103/physrevlett.120.108701
Stewart, I. D. (2011). A systematic review and scientific critique of methodology in modern urban heat island literature. *International Journal of Climatology*, *31*(2), 200–217. https://doi.org/10.1002/joc.2141
Sun, T., Sun, R., & Chen, L. (2020). The trend inconsistency between land surface temperature and near surface air temperature in assessing urban heat island effects. *Remote Sensing*, *12*(8), 1271. https://doi.org/10.3390/rs12081271
Tan, J., Zheng, Y., Tang, X., Guo, C., Li, L., Song, G., et al. (2010). The urban heat island and its impact on heat waves and human health in shanghai. *International Journal of Biometeorology*, *54*(1), 75–84. https://doi.org/10.1007/s00484-009-0256-x
Ukkola, A. M., De Kauwe, M. G., Roderick, M. L., Abramowitz, G., & Pitman, A. J. (2020). Robust future changes in meteorological drought in CMIP6 projections despite uncertainty in precipitation. *Geophysical Research Letters*, *47*, e2020GL087820. https://doi.org/10.1029/2020GL087820
Wan, Z. (2008). New refinements and validation of the MODIS land-surface temperature/emissivity products. *Remote Sensing of Environment*, *112*(1), 59–74. https://doi.org/10.1016/j.rse.2006.06.026
Wang, S., Ju, W., Peñuelas, J., Cescatti, A., Zhou, Y., Fu, Y., et al. (2019). Urban–rural gradients reveal joint control of elevated CO2 and temperature on extended photosynthetic seasons. *Nature Ecology & Evolution*, *3*(7), 1076–1085. https://doi.org/10.1038/s41559-019-0931-1

Ward, H. C., Evans, J. G., & Grimmond, C. S. B. (2013). Multi-season eddy covariance observations of energy, water and carbon fluxes over a suburban area in Swindon, UK. *Atmospheric Chemistry and Physics*, *13*(9), 4645–4666. https://doi.org/10.5194/acp-13-4645-2013

Ward, K., Lauf, S., Kleinschmit, B., & Endlicher, W. (2016). Heat waves and urban heat islands in Europe: A review of relevant drivers. *Science of the Total Environment*, *569–570*, 527–539. https://doi.org/10.1016/j.scitotenv.2016.06.119

Willis, K. J., & Petrokofsky, G. (2017). The natural capital of city trees. *Science*, *356*(6336), 374–376. https://doi.org/10.1126/science.aam9724

Winbourne, J. B., Jones, T. S., Garvey, S. M., Harrison, J. L., Wang, L., Li, D., et al. (2020). Tree transpiration and urban temperatures: Current understanding, implications, and future research directions. *BioScience*, *70*, 576–588. https://doi.org/10.1093/biosci/biaa055

Zeng, Y., Badgley, G., Dechant, B., Ryu, Y., Chen, M., & Berry, J. A. (2019). A practical approach for estimating the escape ratio of near-infrared solar-induced chlorophyll fluorescence. *Remote Sensing of Environment*, *232*, 111209. https://doi.org/10.1016/j.rse.2019.05.028

Zhang, X., Friedl, M. A., Schaaf, C. B., Strahler, A. H., & Schneider, A. (2004). The footprint of urban climates on vegetation phenology. *Geophysical Research Letters*, *31*, L12209. https://doi.org/10.1029/2004gl020137

Zhang, Z., Paschalis, A., & Mijic, A. (2021). Planning London's green spaces in an integrated water management approach to enhance future resilience in urban stormwater control. *Journal of Hydrology*, *597*, 126126.

Zhao, L. (2018). Urban growth and climate adaptation. *Nature Climate Change*, *8*(12), 1034. https://doi.org/10.1038/s41558-018-0348-x

Zhao, L., Lee, X., Smith, R. B., & Oleson, K. (2014). Strong contributions of local background climate to urban heat islands. *Nature*, *511*(7508), 216–219. https://doi.org/10.1038/nature13462

Zhao, L., Oppenheimer, M., Zhu, Q., Baldwin, J. W., Ebi, K. L., Bou-Zeid, E., et al. (2018). Interactions between urban heat islands and heat waves. *Environmental Research Letters*, *13*(3), 034003. https://doi.org/10.1088/1748-9326/aa9f73

Zhou, D., Xiao, J., Bonafoni, S., Berger, C., Deilami, K., Zhou, Y., et al. (2019). Satellite remote sensing of surface urban heat islands: Progress, challenges, and perspectives. *Remote Sensing*, *11*(1), 48.

Zhou, D., Zhao, S., Liu, S., Zhang, L., & Zhu, C. (2014). Surface urban heat island in China's 32 major cities: Spatial patterns and drivers. *Remote Sensing of Environment*, *152*, 51–61. https://doi.org/10.1016/j.rse.2014.05.017

Ziter, C. D., Pedersen, E. J., Kucharik, C. J., & Turner, M. G. (2019). Scale-dependent interactions between tree canopy cover and impervious surfaces reduce daytime urban heat during summer. *Proceedings of the National Academy of Sciences of the United States of America*, *116*(15), 7575–7580. https://doi.org/10.1073/pnas.1817561116